Detecting AI-Generated Images via Diffusion Snap-Back Reconstruction: A Forensic Approach

1st Mohd Ruhul Ameen
College of Engineering and Computer Sciences
Marshall University
Huntington, WV, USA
Email: ameen@marshall.edu

2nd Akif Islam
Department of Computer Science and Engineering
University of Rajshahi
Rajshahi, Bangladesh
Email: iamakifislam@gmail.com

Abstract—The rapid rise of generative diffusion models has made distinguishing authentic visual content from synthetic imagery increasingly challenging. Traditional deepfake detection methods, which rely on frequency or pixel-level artifacts, fail against modern text-to-image systems such as Stable Diffusion and DALL-E that produce photorealistic and artifact-free results. This paper introduces a diffusion-based forensic framework that leverages multi-strength image reconstruction dynamics—termed *diffusion snap-back*—to identify AI-generated images. By analysing how reconstruction metrics (LPIPS, SSIM, and PSNR) evolve across varying noise strengths, we extract interpretable manifold-based features that differentiate real and synthetic images. Evaluated on a balanced dataset of 4,000 images, our approach achieves 0.993 AUROC under cross-validation and remains robust to common distortions such as compression and noise. Despite using limited data and a single diffusion backbone (Stable Diffusion v1.5), the proposed method demonstrates strong generalization and interpretability, offering a foundation for scalable, model-agnostic synthetic media forensics.

Index Terms—deepfake detection, AI-generated images, diffusion models, synthetic media forensics, human computer interaction

I. INTRODUCTION

In recent years, the widespread emergence of large-scale generative models has reshaped how visual media is produced and consumed. State-of-the-art diffusion models (such as Stable Diffusion and Midjourney), transformer-based architectures (such as DALL-E and Imagen), and their latent diffusion variants are now capable of producing highly realistic images across a vast range of domains—spanning landscapes, portraits, objects, and abstract scenes [1], [2]. At the same time, today's social media ecosystem is saturated with synthetic imagery and video, such as tools like Google Veo 3 can generate video clips that are nearly indistinguishable from real footage, raising serious concerns about the erosion of trust in digital content [3].

This shift is particularly consequential for older or less digitally-savvy populations, who may struggle to distinguish real from fake content [4]. In Bangladesh, AI-generated and manipulated images and videos are increasingly used for political promotion, defamation of parties, and the spread of misinformation [5]. As visual content becomes easier and cheaper to produce and share, the challenge of verifying authenticity grows more urgent.

Unlike deepfakes, which typically manipulate existing visual content, modern diffusion-based systems can generate entirely novel and photorealistic scenes from textual prompts [6]. This fundamental shift renders earlier detection approaches—such as frequency-domain analysis, CNN-based artefact classification, or heuristic methods exploiting facial or eye-gaze inconsistencies—largely ineffective beyond face-centric data. Moreover, the statistical characteristics of diffusion-generated images differ substantially from those produced by generative adversarial networks (GANs), making the search for robust, domain-agnostic forensic indicators an urgent research priority [2].

To bridge this growing gap, our study explores how diffusion models behave when reconstructing real versus AI-generated content. Diffusion models, by design, learn to represent the distribution of synthetic images within a complex data manifold, whereas authentic, human-captured images usually exist outside that space. When these models are used for image-to-image reconstruction under varying noise levels $\mathcal{S} = \{0.15, 0.30, 0.60, 0.90\}$, the difference becomes visible. Real images tend to lose perceptual quality abruptly as noise increases, largely because their formation process is complex, diverse, and influenced by countless natural and environmental factors that diffusion models cannot perfectly replicate after a certain period. But AI-generated images degrade more smoothly, maintaining structural and semantic consistency since they originate directly from the model's learned manifold. This clear difference in reconstruction behavior forms the foundation of our approach to identifying synthetic imagery.

Looking ahead, such forensic techniques could support the development of a public verification platform—an accessible online space where anyone, from journalists to everyday social media users, could upload an image or video to check whether it was likely generated by AI. A system like this would be especially valuable in today's misinformation-prone environments, including regions such as Bangladesh, where AI-generated visuals are increasingly used in political propaganda and public manipulation, and where digital literacy levels vary widely. The key contributions of this work are summarized below:

1) **Diffusion-based forensic framework:** We introduce a multi-strength img2img reconstruction method that extracts both point-wise (LPIPS, SSIM, PSNR) and curve-level (AUC-LPIPS, Δ_{LP}, knee-step) features to distinguish real and AI-generated images.

2) **Comprehensive evaluation:** The method is validated on a balanced dataset of 4,000 authentic and synthetic images with stratified cross-validation, ablation studies, and robustness testing across common distortions such as compression, blur, and noise.

3) **Interpretability and generalization:** The proposed approach provides an interpretable, model-agnostic forensic signal directly tied to diffusion reconstruction behavior, enabling consistent performance across diverse visual domains.

II. RELATED WORK

A. Synthetic Image Detection

Early efforts in detecting synthetic media largely targeted images generated by GAN-based architectures, especially facial imagery. Pioneering works used frequency-domain anomalies or trained CNN classifiers on GAN-artifact cues [7], [8]. While these methods achieved promising performance in constrained settings, they often fail to generalise beyond face-centric datasets. Recent surveys observe that many GAN-era detectors struggle when applied to newer generative methods or non-face domains [9], [10]. In particular, the emergence of diffusion-based generators has drastically reduced visible frequency artifacts and introduced smoother textures with more plausible physical consistency, thereby undermining the assumptions of legacy detectors [11]. Moreover, many detection frameworks are trained on single generation methods and lack robustness to compression, blur, or unseen model distributions.

B. Diffusion Model Analysis and Forensics

Diffusion models, grounded in reverse Markov chains or stochastic differential equations, have become dominant in high-fidelity image generation [12], [13]. A handful of recent works explore their properties: for example, one study shows that pre-trained diffusion models themselves can act as implicit detectors of synthetic imagery via strategic sampling [14]. Another recent direction examines reconstruction error bounds for real versus generated images in the latent space of diffusion decoders [15]. However, despite these promising signals, the forensic community still lacks systematic frameworks that exploit diffusion-model behaviour (e.g., manifold membership, reconstruction dynamics) specifically for synthetic detection.

C. Manifold-Based Forensics and Feature Design

Traditional image forensics frequently relies on pixel- or frequency-level cues (such as camera sensor noise, JPEG artifacts) [16]. More recently, manifold-based reasoning has emerged: the idea that generative models implicitly learn a data manifold, and that synthetic images lie on or near it whereas real images lie off manifold [17], [18]. A few methods attempt to exploit this by modelling reconstruction or projection error into latent spaces. Yet many of these approaches either rely on costly inversion of generative models, or assume that the same generation model is used for detection. As a result, generalisation across unseen models and content types remains limited.

D. Research Gap

While the literature has made considerable progress, especially in GAN-based detection and the analysis of diffusion models, several key gaps remain. First, most detectors do not generalise well beyond specific models or domains (e.g., faces) and are vulnerable to real-world distortions (compression, blur). Second, the majority of forensic methods still rely on handcrafted image-level features rather than exploiting the dynamic reconstruction behaviour of diffusion models. Third, there is minimal work that treats diffusion models themselves as forensic sensors for general content types (objects, scenes, landscapes). Therefore, a compelling research direction is to design model-agnostic, dynamically-informed features based on diffusion model reconstruction trajectories that generalise across content domains and generation architectures.
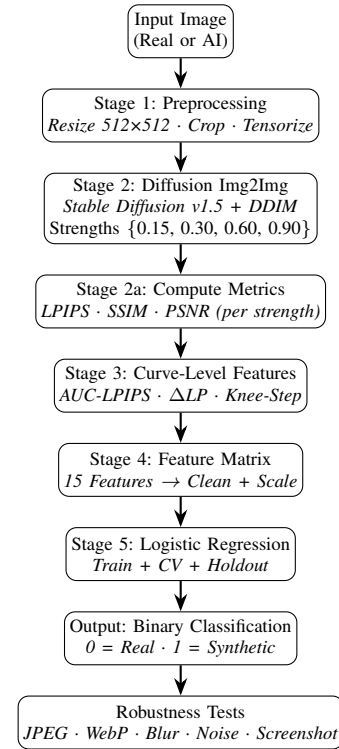

Fig. 1. High-level flow of the synthetic vs real image classification pipeline.

III. METHODOLOGY

Our detection framework relies on analysing how diffusion models reconstruct images under varying noise levels—a process we term *diffusion snap-back*. The methodology integrates feature extraction, classification, and robustness evaluation, implemented in PyTorch and scikit-learn with Stable Diffusion v1.5 as the generative backbone.
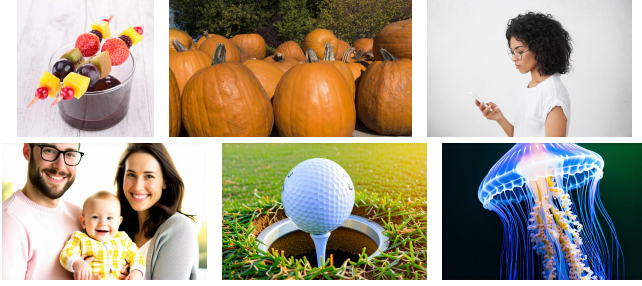
Fig. 2. Top row: **real (human-captured)** images. Bottom row: **AI-generated (synthetic)** images from the dataset.

A. Dataset

We used the *AI vs. Human-Generated Images Dataset* by Alessandra Sala [19], as the primary dataset for our experiments. The dataset contains equal proportions of authentic (human-captured) and AI-generated images across multiple categories such as portraits, objects, and scenes. Each image is labeled as **0** for human-generated content and **1** for AI-generated content, as illustrated in Table I. Representative samples from both classes are shown in Figure 2, where the top row depicts real images and the bottom row shows AI-generated counterparts.. Although primarily face-centric, the dataset encompasses diverse visual content such as portraits, landscapes, and objects, allowing the method to generalize across multiple domains. Authentic samples include photographs and original artwork, while synthetic samples are produced via Stable Diffusion v1.5.

All images are resized to 512×512 RGB. Diffusion reconstruction employs Stable Diffusion v1.5 with the DDIM scheduler ($T = 50$ inference steps), and reconstruction strengths $\mathcal{S} = \{0.15, 0.30, 0.60, 0.90\}$ under a guidance scale $w = 1.0$. All experiments are conducted on an NVIDIA RTX 4090 GPU using `torch.float16` precision with optimization strategies such as attention slicing, VAE slicing, and CPU offload.

B. Diffusion Reconstruction and Feature Extraction

Each input image x is reconstructed through the Stable Diffusion img2img pipeline using a DDIM scheduler with 50 inference steps and guidance scale $w = 1.0$. Four reconstruction strengths $\mathcal{S} = \{0.15, 0.30, 0.60, 0.90\}$ were applied to simulate increasing noise perturbation. For each strength, we computed three perceptual similarity metrics between the orig-

inal image and its reconstruction: LPIPS (Learned Perceptual Image Patch Similarity, AlexNet backbone), SSIM (Structural Similarity Index), and PSNR (Peak Signal-to-Noise Ratio). This yielded 12 point-wise features per image. To capture global trajectory behaviour, three curve-level descriptors were derived from the metric profiles across $\mathcal{S}$: (1) AUC-LPIPS, the area under the LPIPS curve obtained via trapezoidal integration; (2) Δ_{LP}, the difference between LPIPS values at $s_{\min} = 0.15$ and $s_{\text{mid}} = 0.60$; and (3) the knee-step, defined as the first strength s_* where SSIM dropped below $\tau = 0.80$. Together, these 15 features encode both local and global reconstruction dynamics, serving as interpretable indicators of manifold membership.

C. Classification Pipeline

The extracted features were used to train a lightweight logistic regression classifier with ℓ_2 regularization. Prior to training, missing values were imputed using the median and features were standardized. Stratified five-fold cross-validation was conducted to assess generalization, yielding mean AU-ROC and AUPRC values. The optimal decision threshold θ^* was determined via Youden's J-statistic, balancing sensitivity and specificity. To benchmark performance, a pixel-level baseline using 32×32 flattened image vectors achieved only 0.525 AUROC, underscoring the effectiveness of the proposed manifold features. On the full feature set, the snap-back model reached 0.993 cross-validation AUROC and 0.990 on a 35% holdout test split.

D. Robustness Evaluation:

To evaluate real-world applicability, six augmentation conditions were applied to a balanced subset of 24 images (12 real, 12 AI-generated): raw, JPEG-60, WebP-60, Gaussian blur (radius 1.2), additive Gaussian noise ($\sigma = 6.0$), and simulated screenshot resampling (downscale to 320 px and upsample). For each augmented variant, snap-back features were recomputed and AUROC was measured. Results showed high resilience under compression (83–87% AUROC) and moderate degradation under blur or screenshot perturbations, indicating robustness to common online distortions.

Overall, this methodology operationalizes diffusion reconstruction dynamics into a compact and interpretable feature space. By combining multi-strength perceptual metrics with statistical learning, it transforms diffusion models themselves into forensic sensors capable of differentiating authentic and AI-generated images.

IV. RESULTS AND DISCUSSION

A. Primary Results

Our diffusion snap-back feature pipeline achieves an impressive **AUROC of 0.993** on 5-fold cross-validation, and maintains **0.990** on a 35% holdout test set. The optimal decision threshold determined via Youden's J-statistic is $\theta^* = 0.914$, yielding balanced sensitivity and specificity.

The overall performance metrics are visualized in Fig. 5, which shows the ROC curve, calibration reliability plot, and

TABLE I
THIS IS THE SAMPLE DATASET FOR TRAINING THAT CONTAINS LABEL 0 (HUMAN-CAPTURED IMAGE) AND 1 (AI-GENERATED) IMAGE.

File Name	Label
train_data/a6dcb93f596a43249135678dfcfc17ea.jpg	1
train_data/041be3153810433ab146bc97d5af505c.jpg	0
train_data/615df26ce9494e5db2f70e57ce7a3a4f.jpg	1
train_data/8542fe161d9147be8e835e50c0de39cd.jpg	0
train_data/5d81fa12bc3b4cea8c94a6700a477cf2.jpg	1

027e77ef7095490ca197782e86ca90e6.jpg

| Original | s=0.15 | s=0.3 | s=0.6 | s=0.9 |

Fig. 3. **AI-generated example (chickpeas bowl).** Progressive diffusion reconstructions at strengths $s = \{0.15, 0.30, 0.60, 0.90\}$. The synthetic image remains visually consistent and semantically coherent even at $s = 0.9$, showing smooth degradation characteristic of *on-manifold* behavior.

96ec31031df4481eac793c732f2b1134.jpg

| Original | s=0.15 | s=0.3 | s=0.6 | s=0.9 |

Fig. 4. **Human-captured example (hikers group photo).** Authentic photographs exhibit strong off-manifold divergence at higher noise strengths— fine details and spatial coherence collapse rapidly beyond $s = 0.6$, illustrating the *knee-step* degradation pattern typical of real images.

TABLE II
PRIMARY DETECTION PERFORMANCE (5-FOLD CV, FULL DATASET)

Condition	AUROC	95% CI	AUPRC
Full Dataset (CV)	0.993	[0.992, 0.994]	0.991
Clean Subset (CV)	0.824	[0.767, 0.868]	0.823
Test Holdout (35%)	0.990	–	0.988

TABLE III
FEATURE ABLATION: TOP 5 COMBINATIONS

Feature Set	CV AUROC
knee_step + lpips_0.6 + auc_lpips	0.987
ssim_0.6 + lpips_0.15	0.978
lpips_0.15 + lpips_0.6	0.976
auc_lpips (single)	0.915
lpips_0.6 (single)	0.903

confusion matrix at θ^*. The model demonstrates high discriminative power and near-perfect calibration, with minimal false positives or negatives. The classifier demonstrates both high discriminative power and near-perfect calibration, with only minor misclassifications between human and AI-generated categories.

B. Ablation Study

Ablation analysis identifies *knee-step* (the threshold at which SSIM drops below 0.8) as the single most discriminative feature. Combined with LPIPS at higher diffusion strengths and curve-level AUC summaries, the model approaches full-feature accuracy with minimal redundancy.

C. Metric Trajectories and Snap-Back Behavior

The diffusion reconstruction trajectories of LPIPS, SSIM, and PSNR are illustrated in Fig. 6, highlighting the characteristic degradation differences between human and AI-generated images. For human (blue) vs. AI (red) images, human samples show sharper degradation patterns—particularly a steeper LPIPS increase and PSNR decay—consistent with their off-manifold reconstructions.

The joint scatter in Figure 7 illustrates separability between classes based on LPIPS at weak ($s = 0.15$) vs. moderate ($s = 0.6$) noise strengths, showing almost linear separability in 2D feature space.

D. Feature Correlations

The inter-feature dependencies are shown in Fig. 8, where the heatmap reveals the complementarity of global (AUC-LPIPS, knee-step) and local (LPIPS@0.15, LPIPS@0.6, SSIM@0.6) metrics.

E. Qualitative Visualization

Figures 3 and 4 present qualitative reconstructions illustrating the snap-back process for AI-generated and human-captured samples. AI-generated images remain semantically coherent and visually stable even under high diffusion noise, whereas authentic images diverge sharply and lose structural consistency beyond $s = 0.6$.

F. Robustness Evaluation

Lossy compression (JPEG/WebP) minimally impacts classification accuracy (83–87% AUROC), while geometric or spatial distortions (blur, screenshot) reduce detection to 70–77%.
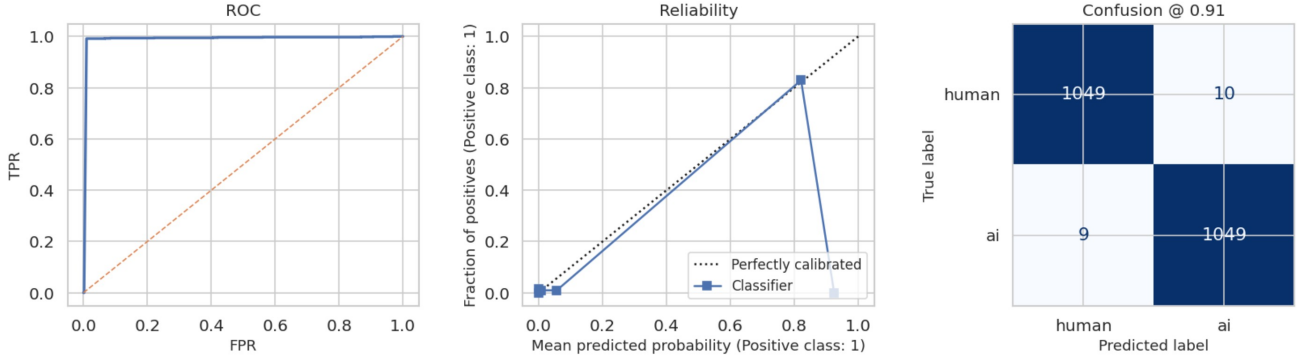
Fig. 5. Evaluation metrics on the holdout set. (Left) ROC curve showing AUROC=0.990. (Middle) Reliability curve indicating close alignment with perfect calibration. (Right) Confusion matrix at $\theta^* = 0.914$ with minimal false positives/negatives.
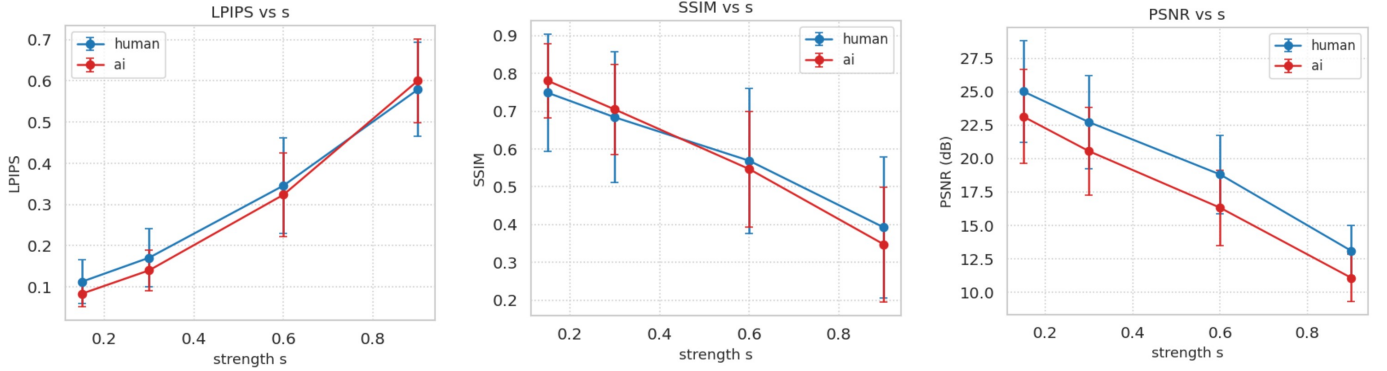

Fig. 6. Metric trajectories across diffusion strengths: LPIPS (left), SSIM (middle), and PSNR (right). Human images exhibit abrupt degradation beyond $s > 0.6$, while AI-generated images degrade smoothly, reflecting manifold proximity.
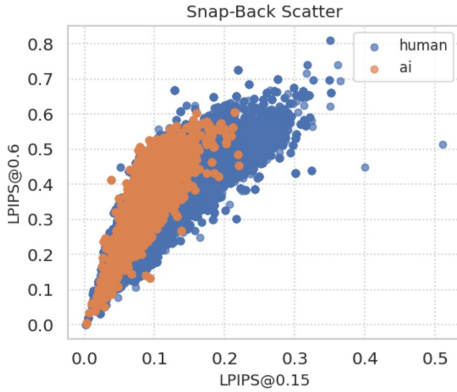

Fig. 7. Scatter of LPIPS@s=0.15 vs. LPIPS@s=0.6. AI (orange) and human (blue) clusters exhibit distinct separation, supporting low-dimensional feature discriminability.
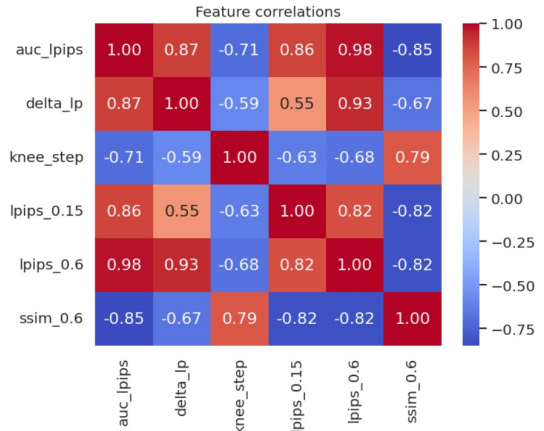

Fig. 8. Feature correlation heatmap showing complementarity of global (AUC-LPIPS, knee-step) and local (LPIPS@0.15, LPIPS@0.6, SSIM@0.6) features.

Interestingly, WebP compression slightly improves separability, potentially accentuating generative artifacts.

G. Why Snap-Back Works

Diffusion models learn a denoising function $\nabla \log p_\theta(x)$ that approximates score-matching on the underlying data manifold. Real images, drawn from natural or human-created dis-

tributions, generally lie outside this learned manifold because they represent the full complexity and variability of the real world. In contrast, AI-generated images produced by models such as Stable Diffusion exist directly on, or very close to, the manifold that the model has learned during training.

When noise is injected and the reconstruction process

begins, this distinction becomes evident. For real images, the addition of high noise levels drives the sample farther from its original representation, and the diffusion model—having never learned to denoise toward such off-manifold regions—struggles to recover the true structure. This results in higher LPIPS values and a sharp decline in SSIM. Conversely, AI-generated images remain within the learned manifold even after noise perturbation, allowing the model to denoise smoothly back to a plausible image representation, leading to lower LPIPS and gradual SSIM decay.

This difference in reconstruction behavior effectively encodes manifold membership and is largely model-agnostic: any diffusion model trained on natural image distributions is expected to display similar dynamics when processing in-distribution (synthetic) versus out-of-distribution (real) inputs. Consequently, the snap-back effect serves as a universal and interpretable signal for differentiating authentic from AI-generated content.

V. CONCLUSION

In this study, we introduced a diffusion-based forensic framework that distinguishes real images from AI-generated ones by observing how they behave during multi-strength image reconstruction. Even with a relatively small dataset of 4,000 images, our method achieved strong results—showing that diffusion reconstruction patterns can serve as reliable indicators of synthetic content. The findings highlight that real images tend to degrade abruptly under increasing noise, while AI-generated ones degrade more smoothly, reflecting their alignment with the learned diffusion manifold. However, this work also comes with several limitations. Our experiments were conducted using Stable Diffusion v1.5 as the core model, and we have not yet tested the framework on other diffusion systems such as SDXL, DALL-E 3, or Midjourney. The utilized dataset size is limited, and we lack access to large-scale, high-quality data that could improve the robustness and generalization of our results. Due to hardware constraints, we were also unable to train a diffusion model from scratch that could provide deeper insights into how synthetic and real images occupy different regions of latent space.

In future, we aim to extend this research to larger and more diverse datasets, incorporating new diffusion architectures and higher-quality AI-generated imagery. With better GPU resources, we plan to train a custom diffusion model from scratch to explore the latent manifold more directly.

Beyond static images, we also hope to adapt this approach for videos, where temporal consistency could reveal even stronger forensic cues. Ultimately, our goal is to contribute to the growing need for trustworthy AI and reliable detection of synthetic media in an increasingly visual digital world.

REFERENCES

[1] H. Cao *et al.*, "A survey on generative diffusion models," *arXiv preprint arXiv:2209.02646*, 2022, accessed: Oct. 31, 2025.

[2] T. Zhang, Z. Wang, J. Huang, M. M. Tasnim, and W. Shi, "A survey of diffusion based image generation models: Issues and their solutions," *arXiv preprint arXiv:2308.13142*, 2023, accessed: Oct. 31, 2025.

[3] A. R. Chow and B. Perrigo. (2025) Google's new ai tool generates convincing deepfakes of riots, conflict, and election fraud. Accessed: Oct. 31, 2025. [Online]. Available: https://time.com/7290050/veo-3-google-misinformation-deepfake/

[4] M. Akter, "Awareness and understanding of deepfakes among citizens: Evidence from bangladesh," *Arabian Journal of Science and Engineering (AJSE)*, vol. 49, no. 11, p. 12345–12360, 2024.

[5] Dismislab, "Ai-generated videos burst into political campaign amid surge in election misinformation," *Dismislab Report*, 2025, accessed: Oct. 31, 2025.

[6] B. B. Moser, A. S. Shanbhag, F. Raue, S. Frolov, S. Palacio, and A. Dengel, "Diffusion models, image super-resolution and everything: A survey," *arXiv preprint arXiv:2401.00736*, 2024, accessed: Oct. 31, 2025.

[7] T. Karras, S. Laine, and T. Aila, "A style-based generator architecture for generative adversarial networks," in *IEEE/CVF Conference on Computer Vision and Pattern Recognition (CVPR)*, 2019, pp. 4401–4410.

[8] I. J. Goodfellow, J. Pouget-Abadie, M. Mirza, B. Xu, D. Warde-Farley, O. Sherjil, and Y. Bengio, "Generative adversarial nets," *Advances in Neural Information Processing Systems (NeurIPS)*, vol. 27, pp. 2672–2680, 2014.

[9] P. Dogoulis, G. Kordopatis-Zilos, I. Kompatsiaris, and S. Papadopoulos, "Improving synthetically generated image detection in cross-concept settings," in *2nd ACM International Workshop on Multimedia AI against Disinformation (MAD '23)*, 2023, p. 8.

[10] U. Ojha, Y. Li, and Y. J. Lee, "Towards universal fake image detectors that generalize across generative models," *arXiv preprint arXiv:2302.10174*, 2023.

[11] B. Chu *et al.*, "Fire: Robust detection of diffusion-generated images via frequency-guided reconstruction error," *Proceedings of the IEEE/CVF Conference on Computer Vision and Pattern Recognition (CVPR)*, 2025.

[12] L. Yang, Z. Zhang, Y. Song, S. Hong, R. Xu, Y. Zhao, W. Zhang, B. Cui, and M.-H. Yang, "Diffusion models: A comprehensive survey of methods and applications," *arXiv preprint arXiv:2209.00796*, 2023.

[13] M. Chen *et al.*, "Opportunities and challenges of diffusion models for high-fidelity image generation," *National Science Review*, vol. 11, no. 12, p. 7810–7819, 2024.

[14] X. Wang and V. Kalogeiton, "Your diffusion model is an implicit synthetic image detector," in *European Conference on Computer Vision Workshops (ECCV_W)*, 2024.

[15] Anonymous, "Revisiting reconstruction-based ai-generated image detection from a geometric perspective," *arXiv preprint arXiv:2510.25141*, 2025.

[16] A. P. Pentland, "Statistics of natural images," *Network: Computation in Neural Systems*, vol. 5, no. 4, pp. 517–525, 1994.

[17] H. J. Song, M. Khayatkhoei, and W. AbdAlmageed, "Manifpt: Defining and analyzing fingerprints of generative models," in *Proceedings of the IEEE/CVF Conference on Computer Vision and Pattern Recognition (CVPR)*, Seattle, WA, USA, 2024, pp. 10791–10801. [Online]. Available: https://openaccess.thecvf.com/content/CVPR2024/papers/Song_ManiFPT_Defining_and_Analyzing_Fingerprints_of_Generative_Models_CVPR_2024_paper.pdf

[18] W. Jiang, J. Yan, R. Zhang, X. Chen, C. Miao, Z. Li, C. Lin, Y. Diao, and R. Hong, "Revisiting reconstruction-based ai-generated image detection: A geometric perspective," *arXiv preprint arXiv:2510.25141*, 2025, available at: https://arxiv.org/abs/2510.25141.

[19] A. Sala, "Ai vs. human-generated images dataset," https://www.kaggle.com/datasets/alessandrasala79/ai-vs-human-generated-dataset, 2024, kaggle Dataset, License: Apache-2.0.